Controllable Crystallite and Particle Sizes of WO_3 Particles Prepared by a Spray-Pyrolysis Method and Their Photocatalytic Activity

Osi Arutanti and Takashi Ogi
Dept. of Chemical Engineering, Graduate School of Engineering, Hiroshima University, 1-4-1 Kagamiyama, Higashi Hiroshima 739-8527, Japan

Asep Bayu Dani Nandiyanto
Dept. of Chemical Engineering, Graduate School of Engineering, Hiroshima University, 1-4-1 Kagamiyama, Higashi Hiroshima 739-8527, Japan

Dept. Kimia, Fakultas Pendidikan Matematika dan Ilmu Pengetahuan Alam, Universitas Pendidikan Indonesia, Jl. Dr. Setiabudhi No. 229 Bandung 40154, Indonesia

Ferry Iskandar
Dept. of Physics, Institut Teknologi Bandung, Jl. Ganesha No. 10 Bandung 40132, Indonesia

Kikuo Okuyama
Dept. of Chemical Engineering, Graduate School of Engineering, Hiroshima University, 1-4-1 Kagamiyama, Higashi Hiroshima 739-8527, Japan

DOI 10.1002/aic.14233
Published online November 11, 2013 in Wiley Online Library (wileyonlinelibrary.com)

Information about correlation of material properties parameters (i.e., crystallite and particle sizes) and photocatalytic activity of tungsten trioxide (WO_3) particles are still lacking. For this reason, the purpose of this study was to synthesize WO_3 particles with controllable crystallite (from 18 to 50 nm) and particle sizes (from 58 to 677 nm) using a spray-pyrolysis method and to investigate correlation of crystallite/particle size and photocatalytic activity. To gain control of crystallite/particle size, synthesis temperature (120–1300°C) and initial precursor concentration (2.5–15 mmol/L) were investigated, which were then compared with the proposal of the particle formation mechanism. The results showed that both crystallite and particle sizes played an important role in photocatalytic activity. In this research, the optimum condition to produce the highest photocatalytic performance of WO_3 particles was at the temperature of 1200°C (crystallite size: 25 nm), and initial concentration of 10 mmol/L (particle size: 105 nm). © 2013 American Institute of Chemical Engineers *AIChE J*, 60: 41–49, 2014
Keywords: nanoparticle, photocatalyst, spray-pyrolysis, ammonium tungstate pentahydrate, crystal

Introduction

Tungsten trioxide (WO_3) is one of the most prospective catalysts because it possesses many excellence properties (e.g., good photostability, excellent absorption of solar radiation (visible light), biologically and chemically inert, good thermal stability, etc).[1,2] However, there are several problems regarding to availability and price of WO_3.[3] For this reason, preparation of WO_3 material with high-photocatalytic activity and lower tungsten usage is inevitable.[4–10]

To produce WO_3 material with excellent performances, many methods have been reported. However, most of the current reports are in film form,[2] while reports in the synthesis of particles are typically less. In fact, implementation of photocatalyst films in large-scale industrial processes is difficult. For circumventing the problems associated with the production of WO_3 particles, several methods have been suggested, including sol–gel, hydrothermal, chemical vapor deposition, sputtering, and anodic oxidation.[4,7,9,11,12] Although their methods are able to produce particles, most reports described successful production of particles with only partial information on controlling crystallite and particle sizes, as well as their impact on photocatalytic activity.

Information about correlations between material properties parameter (i.e., crystallite and particle sizes), and photocatalytic activity of WO_3 particles are still lacking. Most reports did not discriminate the influence of "crystallite with a constant particle size" or "particle size with a constant crystallite size" on photocatalytic activity. In fact, investigation of WO_3 particles with controllable crystallite and particle sizes is important.

Additional Supporting Information can be found in the online version of this article.

Correspondence concerning this article should be addressed to T. Ogi at ogit@hiroshima-u.ac.jp.

© 2013 American Institute of Chemical Engineers

In our previous studies, we synthesized WO_3 particles with controllable particle size,[13] composition (adding Pt dopant),[14] and porous structure.[3] However, we did not report in detail about the influence of crystallite size yet. Here, the purpose of this study was to synthesize WO_3 particles with controllable crystallite and particle sizes and to investigate the correlation of crystallite/particle size and photocatalytic activity.

To produce WO_3 particles, we used a spray-pyrolysis method because this method can produce agglomeration-free particles.[15,16] Thus, the effect of crystallite and particle sizes on photocatalytic performance can be investigated precisely. We selected ammonium tungstate pentahydrate (ATP) as a model for WO_3 source because conversion of this chemical into WO_3 is free of impurities.[3] Detailed investigation of the effect of synthesis temperature and precursor concentration was also presented along with the proposal of the particle formation mechanism, in which this information is typically disregarded in the current WO_3 particle synthesis reports. Interestingly, this method was effective to control crystallite and particle size only by changing synthesis temperature and precursor concentration. To support our study, we used electron microscopes, X-ray diffraction, nitrogen sorption, and thermal analysis.

We also investigated the effect of crystallite and particle sizes on photocatalytic performance. As a model for organic waste, we used rhodamine B (RhB). RhB had high photostability and water solubility rather than other dyes (e.g., methylene blue), making this chemical difficult to be degraded using conventional wastewater treatment methods. RhB is also one of the most used dyes in industrial applications, making that the successful treatment of this chemical can be directly applied for realistic applications. The result showed that both crystallite and particle sizes played an important role in photocatalytic activity in degrading RhB. We also optimized the process for gaining high performance of photocatalyst, which is useful for synthesis of particles particularly with a view to screening and enhancing the material properties.

Experimental Method

Synthesis of WO_3 particles

To synthesize WO_3 particles, ATP ($(NH_4)_{10}(W_{12}O_{41}).5H_2O$; purity 88–90%; Kanto Chemical Co., Inc., Japan) was used and diluted into ultra-pure water (UPW). The diluted ATP (namely the precursor) was then put into the particle production system, shown in Figure 1. This reactor system consist of an ultrasonic nebulizer (NE-U17; Omron Healthcare Co., Ltd., Japan; operated at 1.7 MHz; to generate droplet), a tubular ceramic reactor (1.3 m in length and 30 mm in inner dia.), and an electrostatic precipitator (10,000 V; 120°C). Detailed electrostatic precipitator is described in detail in our previous work.[17] To introduce the generated droplet into the tubular furnace, we used a flow of carrier gas (air; 5 L/min). To produce particles with controllable crystallite and particle sizes, we varied the synthesis temperature (from 120 to 1300°C), and the initial precursor concentration (from 2.5 to 15 mmol/L).

Characterizations

The morphology of the prepared particles were examined using a scanning electron microscope (SEM, Hitachi S-5000, Japan; operated at 20 kV), and a transmission electron microscope (TEM, JEM-3000F, Japan; operated at 300 kV). An X-ray diffraction (XRD; RINT2000 V, Rigaku Denki, Japan; using Cu Kα radiation ($\lambda = 1.54$ Å); operated at 40 kV and 30 mA with a scan step of 0.02°) was used to evaluate the crystal structure. To determine the specific surface area, a nitrogen adsorption analysis (BET; BELSORP 28SA; Bel Japan, Japan) was used. We also analyzed sample using a thermogravimetric and differential thermal analyzer (TG-DTA; Exstar6000, Seiko Instruments, Inc., Japan; heating rate = 5°C/min; carrier gas: air, 200 mL/min).

To investigate the photocatalytic activity of the prepared particles, the photodecomposition of RhB under solar irradiation (PEC—L11, Peccell Technologies, Inc., Japan; AM 1.5G (100 mW/cm^2)) was measured. For simplification the photodecomposition process used: 2 ppm of aqueous solution of RhB, 200 mg of prepared particles, and 500 mL of UPW. To maintain concentration dissolved oxygen in the solution, 200 mL/min of oxygen gas was bubbled into the reactor. Detailed photodegradation system is described in our previous work.[3] To measure the concentration of remained RhB, sample was taken and analyzed using a UV–vis spectrophotometer (UV3150, Shimadzu, Japan; evaluated in the wavelength range of 400–700 nm at room temperature).

Results and Discussions

Effect of synthesis temperature on physicochemical of WO_3 properties

To investigate the effect of synthesis temperature on particles formation precisely, we used precursor with concentration of 10 mmol/L because this concentration is appropriate to produce submicron particles, based on our previous work[3]. Too high concentration has problems in the ATP solubility in water, whereas too low-precursor concentration caused less production rate.

Figure 2 shows the XRD patterns of spray-pyrolyzed particles prepared with various synthesis temperatures (600 to 1300°C). The XRD patterns suggested that the prepared particles had two types of crystal structures: hexagonal (JCPDS no. 75–2187) and monoclinic (JCPDS no. 72–1465). The hexagonal structure was prepared at a synthesis temperature of around 600°C. A mixture of monoclinic and hexagonal structures was formed at higher synthesis temperatures from 700–1050°C. The crystal structure changed to hexagonal structure at temperature of above 1050°C. From the Scherer equation, the crystallite size increased from 18 to 41 nm with the increasing of synthesis temperatures from 600 to 1000°C. The crystallite sizes were 37, 29, 25, and 23 nm in corresponding to the synthesis temperature of 1050, 1100, 1200, and 1300°C, respectively.

Figure 3 shows the SEM images of the particles prepared at various synthesis temperatures from 600 to 1300°C. In the range of 600 and 1000°C, the prepared particles were in spherical shape with a mean particle size of about 600 nm (Figure 3a–e). The increasing of temperature further to 1050°C led the decreasing in particle size to around 488 nm (Figure 3f). The size of the prepared particles greatly decreased to 177 nm, 105 nm, and 87 nm, corresponding to the synthesis temperature of 1100, 1200, and 1300°C, respectively (Figure 3g–i).

Figure 4 shows the TEM analysis of particles prepared at various synthesis temperatures (from 700 to 1300°C). Figure

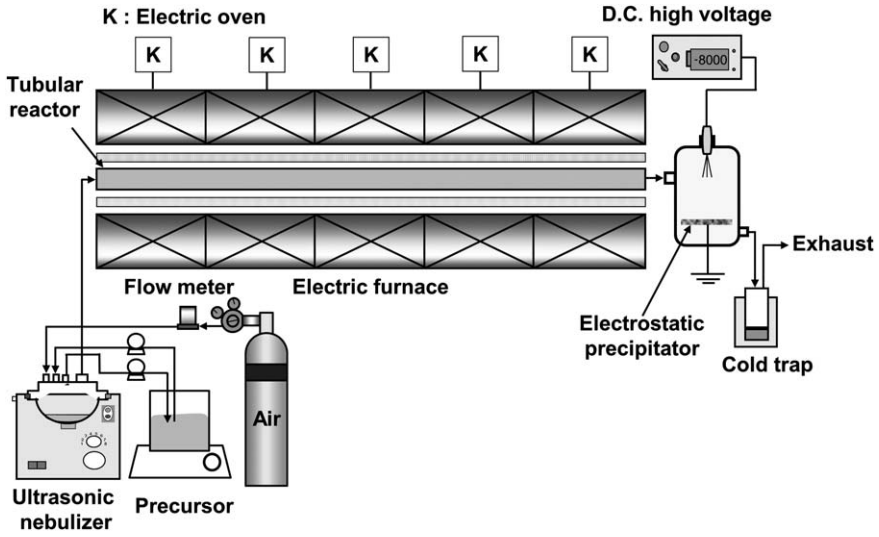

Figure 1. Schematic illustration of experimental setup.

4a shows that when using a synthesis temperature of 700°C, particles with a spherical shape are produced. The observation of outer morphology gained by TEM results were in a qualitative agreement with the SEM results in Figure 3b. When the temperature was increased to 800°C, particles with a rough surface were generated (Figure 4b). As the calcination temperature was increased to 900°C, incomplete spherical particles with a highly faceted shape were produced (Figure 4c). The use of higher synthesis temperatures, changes in the particle morphology were observed (Figure 4d–e). Synthesis temperatures of 1200 and 1300°C gave the creation of hexagonal shaped nanoparticles. The lattice fringe spacing of WO_3 particles was 5.18; 4.62; 5.05; 5.17; and 5.03 Å, corresponding to synthesis temperatures 700, 800, 900, 1200 and 1300°C, respectively.

To clarify the structure inside the particles, a nitrogen adsorption analysis was conducted shown in Figure S1 online in the Supporting Information. The analysis showed that all particles exhibited a characteristic type-II isotherm (Figure S1a), indicating the prepared particles were nonporous. The Barrett-Joyner-Halenda (BJH) method was also confirmed that no micro- and mesoporous structures were identified in all samples, as shown in Figure S1b.

In the range of 600–1000°C, increase in synthesis temperature causes increase in the material crystallization, indicated by the increase in crystallite size due to the same initial concentration of ATP. However, there is no significant change in the particle size. Further increases in the temperature cause the modification of particle outer shape. This result confirms that the higher-temperature process causes the more additional energy supply for improving crystallite growth. Thus, the higher temperature leads the production of particles with larger crystallite size.

In addition, anomaly results were found for the case of particles prepared using temperatures of above 1000°C. The particle sizes decrease drastically and there is a modification in the crystal structure. WO_3 material seems to be evaporated during the process. Then, when the evaporated WO_3 components are cooled (contacting temperature of below than 1000°C), they are reconstructing, reassembling, and coalescing to form stable crystal condition. Thus, the particles with different crystal structures are formed in the final product. Due to the limitation for the cooling time process, the particles with nanometer sizes are produced.

The possible mechanism of WO_3 particle formation during the spray-pyrolysis method is shown in Figure 5. We divided the mechanism in two parts (1) pretreatment (<600°C), and (2) crystallization (600–1300°C).

In the pretreatment process, the main principle of this step is to deliver and rapidly heat an initial solution/slurry via the direct injection of very small droplets.[22] Droplets are generated from the atomization of precursor using ultrasonic nebulizer, in which these droplets are then introduced into the

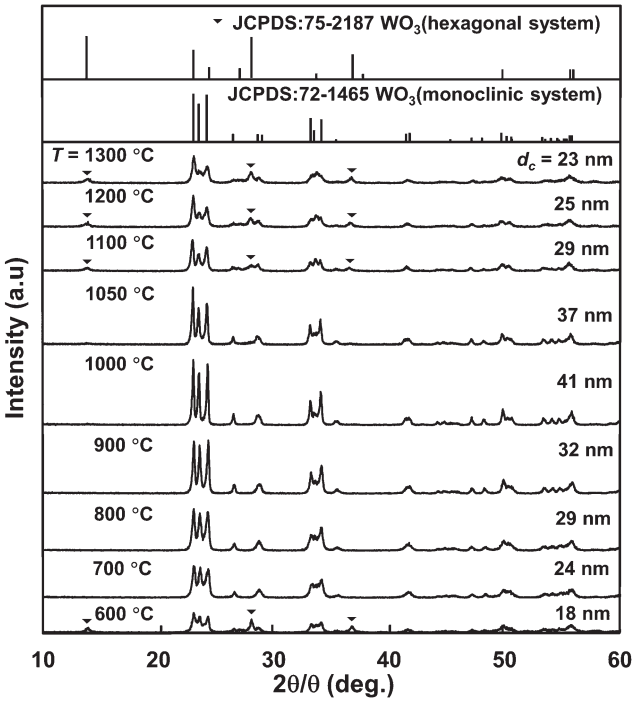

Figure 2. XRD patterns of particles prepared with various synthesis temperatures at constant initial concentration of 10 mmol/L.

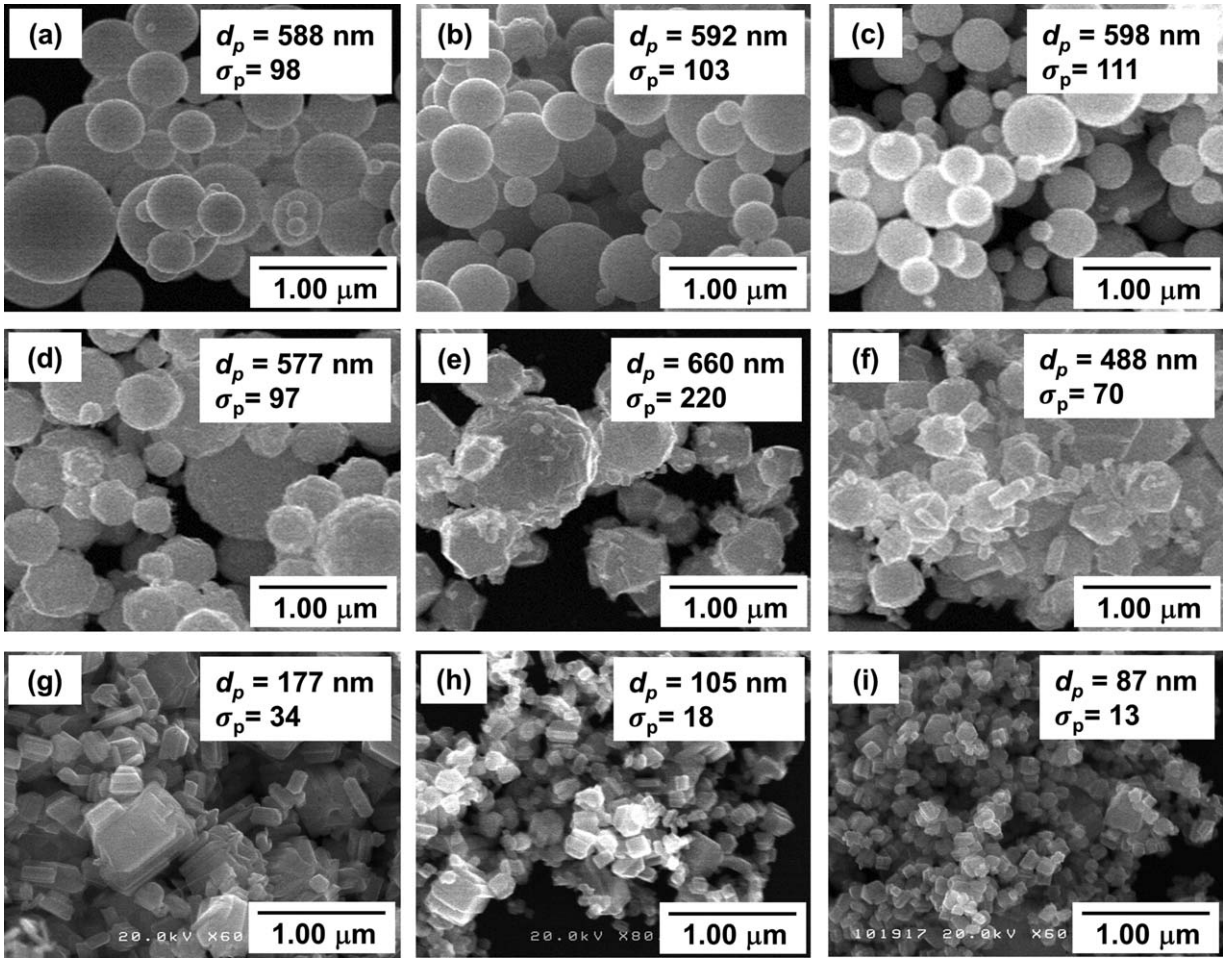

Figure 3. SEM images of particles prepared at various synthesis temperatures (a) 600, (b) 700, (c) 800, (d) 900, (e) 1000, (f) 1050, (g) 1100, (h) 1200, and (e) 1300°C. Particles were produced using 10 mmol/L of ATP.

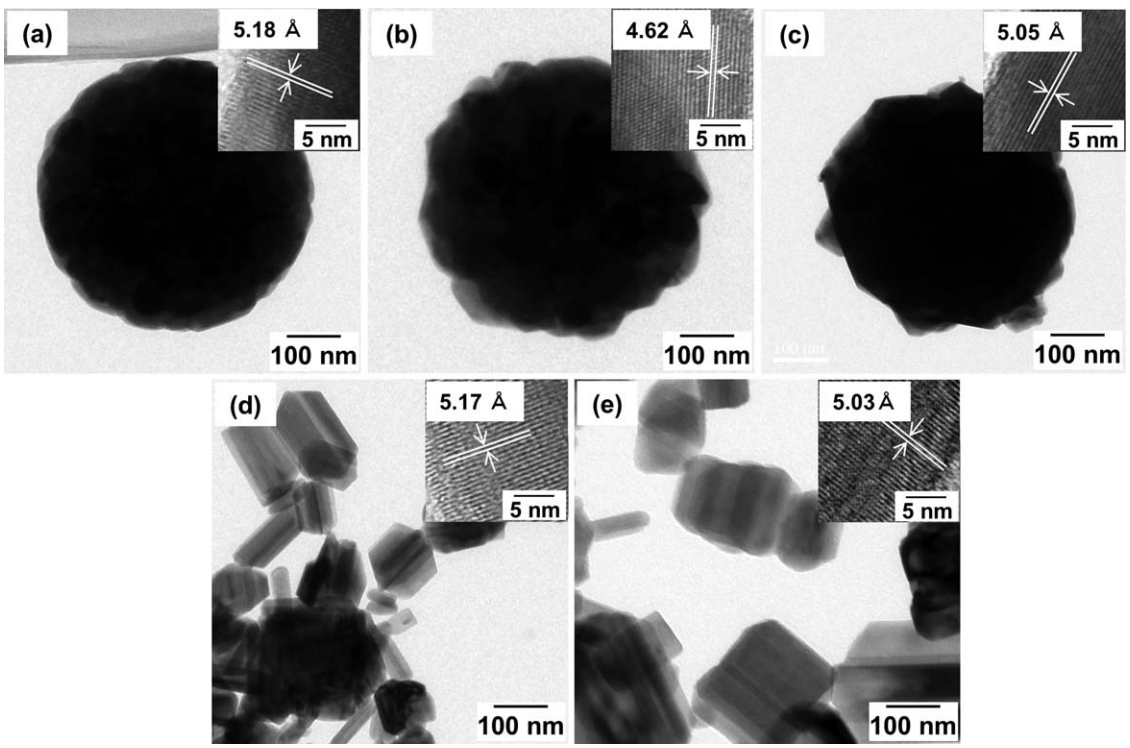

Figure 4. TEM images of particles prepared with precursor concentration of 10 mmol/L ATP under different synthesis temperatures (a) 700, (b) 800, (c) 900, (d) 1200, and (e) 1300°C.

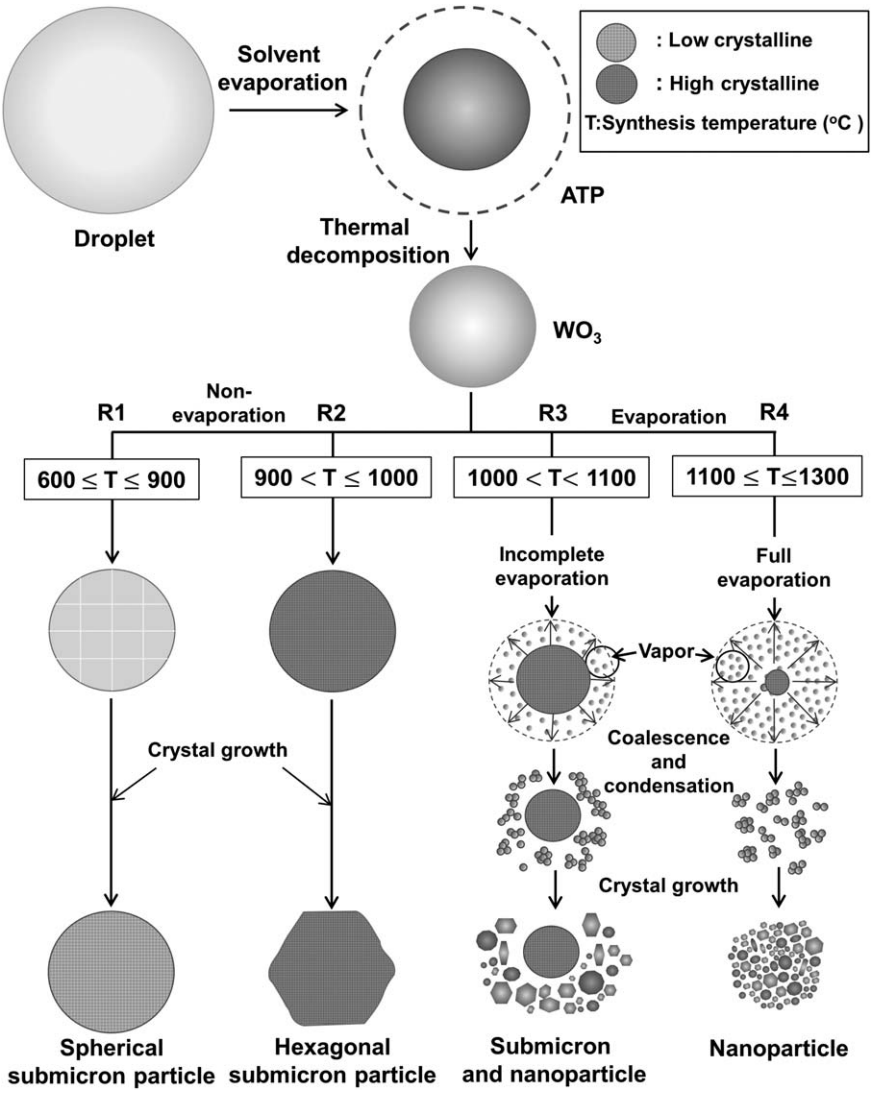

Figure 5. Mechanism of the formation of particles in spray-pyrolysis method as the effect of various synthesis temperatures.

heated reactor. Contacting droplets with temperature of 120–300°C, solvent evaporates. Further additional temperature, thermal decomposition of ATP occurs, producing amorphous WO_3 particles. With the increase of temperature (400–600°C), these amorphous particles transform into higher crystalline WO_3 particles. Detailed explanation in the pretreatment process (including reaction mechanism and physicochemical analysis, photograph images, thermal analysis, and XRD pattern) are described in Figure S2–S5 in the Supporting Information.

In the crystallization zone, there are two phenomena. One is particle synthesis with non-evaporation process (600–1000°C), and the other is particle synthesis with evaporation process (>1000°C).

The first phenomena are shown in route R1 and R2. Route R1 in Figure 5 is the formation of spherical submicron particles. This can be obtained when the process is at temperature of below than 900°C. Adding a higher-temperature process (between 900 and 1000°C) leads the production of submicron aspherical particles with faceted shapes (route R2).

When applying crystallization process with temperatures of higher than 1000°C, second phenomena happen (shown in route R3 and R4). WO_3 material evaporates. When using temperature of between 1000 and 1100°C, incomplete evaporation happens (route R3). As a result, particles with a broad size distribution are prepared. When using temperature of higher than 1100°C (route R4), all products are nanoparticles.

Effect of Initial Precursor Concentration

To investigate the effect of initial concentration on particle size and morphology, we selected the synthesis temperature of 900 and 1200°C, in which these temperatures can be used as a model for synthesis process with evaporation and non-evaporation phenomena, respectively.

Figure 6 shows the SEM images of particles prepared with various initial precursor concentrations at 900°C. Submicron particles with a spherical shape were obtained for all cases. Particles sizes increased with increasing precursor concentration. The Ferret diameters of particles (shown in Figure 6a–d) were 388, 454, 579, and 767 nm, corresponding to initial precursor concentrations of 2.5, 5, 10, and 15 mmol/L, respectively.

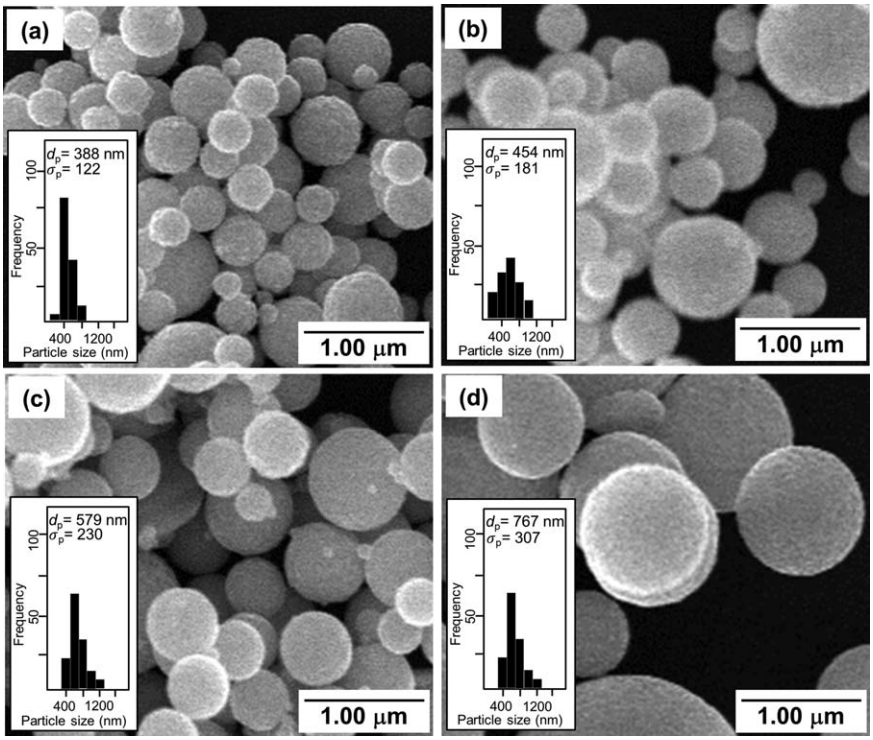

Figure 6. SEM images of particles prepared with various initial precursor concentrations (a) 2.5, (b) 5, (c) 10, and (d) 15 mmol/L at 900°C.

Particles were produced using 10 mmol/L of ATP.

Figure 7 shows the SEM images of particles prepared with various precursor concentrations at 1200°C. A strong correlation between precursor concentration and particle size was obtained. Increases in precursor concentration affected the increases in particle size. In addition, we also found that the precursor concentration modify particle shape.

When using the precursor concentration of 2.5 mmol/L, spherical particles with a mean size of 58 nm were produced (Figure 7a). When the precursor concentration was increased

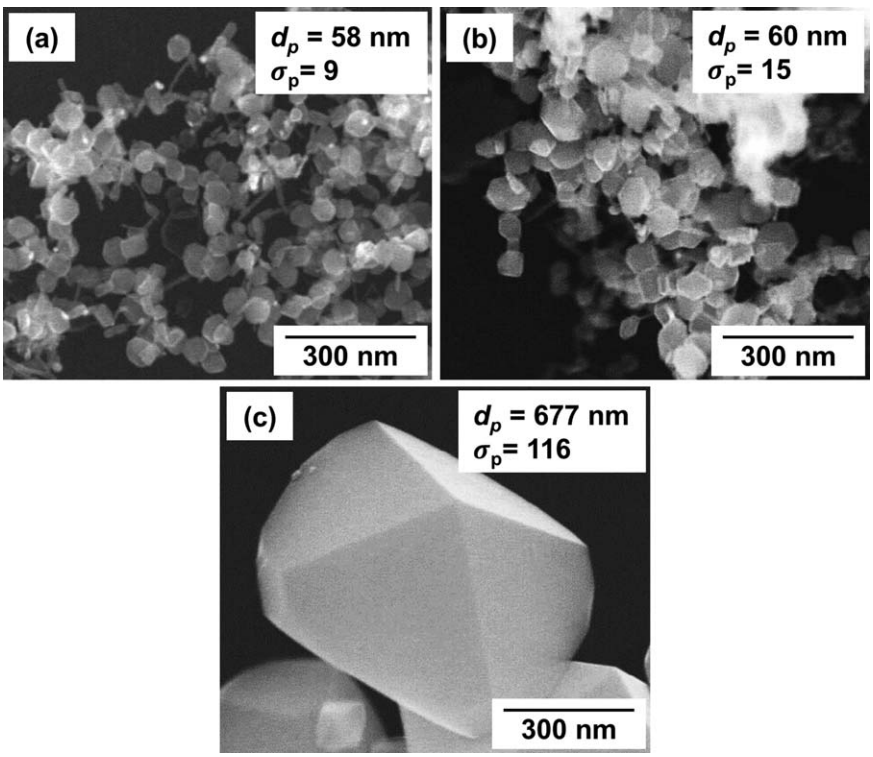

Figure 7. SEM images of particles prepared with various initial precursor concentrations under synthesis temperature at 1200°C (a) 2.5, (b) 5, and (c) 15 mmol/L.

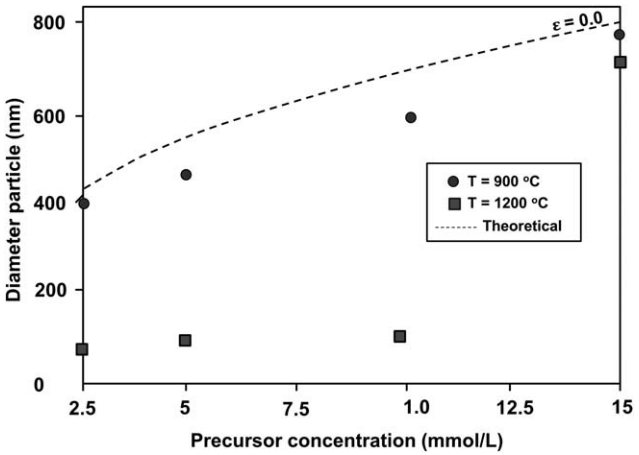

Figure 8. Comparison of the particle diameter between experimental and theoretical calculation.

to 5 mmol/L, a mean particle size increased to 60 nm (Figure 7b). By increasing the precursor concentration to 15 mmol/L, particles with a diamond like shape and a mean size of 677 nm were created (Figure 7c).

In addition, we found interesting result. From the aforementioned experimental results in Figures 6 and 7, XRD patterns of sample in Figure 6 shows there is no change in XRD phase and pattern. However, XRD patterns from sample in Figure 7 shows the occurrence of changes in pattern and crystallite size (18 to 50 nm). This change is due to the particle evaporation at high temperature as shown in Figure 5. All data are presented in the Supporting Information (Figures S6 and S7).

Figure 8 shows effect of precursor concentration on particle size in detail with theoretical calculation result. Experimental results are shown by "solid dot" for synthesis temperature of 900°C and "solid square" for synthesis temperature of 1200°C, whereas the theoretical calculations are shown by "dashed line". The theoretical calculation is gained using the following equation[15]

$$D_p = D_D C_D \left(\frac{1}{(1-\varepsilon)} \sum \frac{M_i . C_i}{\rho_i} \right)^{1/3} \quad (1)$$

where D_p is the mean diameter of the prepared particle (μm), D_d is the mean diameter of the mean diameter of droplet (μm), C_D is the constant (0.0464), and ε is the particle porosity. M is the molecular weight, C is the initial concentration (g/L), and ρ is the density (g/mL). In the ultrasonic nebulizer, generated droplet diameter (D_d) is 4.5 μm.

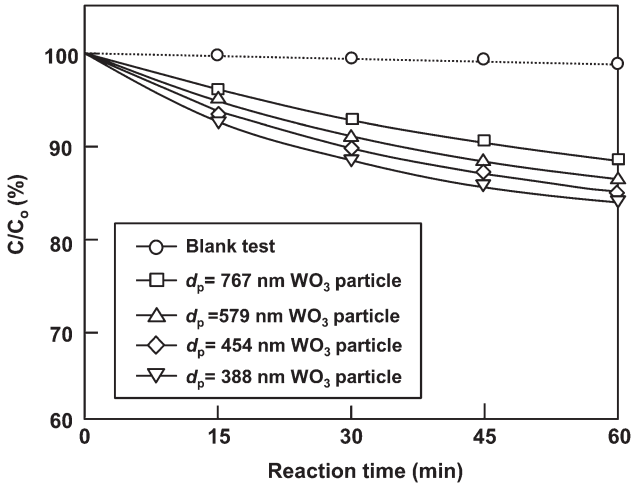

Figure 9. Photodegradation of RhB by WO_3 particles with various particle sizes.

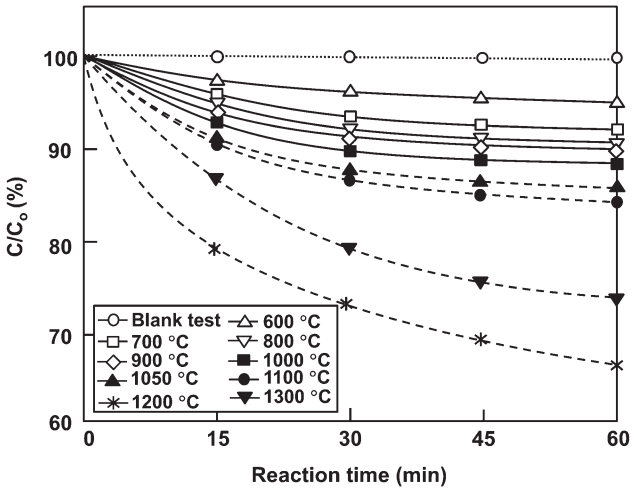

Figure 10. Photodecomposition of RhB by WO_3 particles with various crystal sizes.

The results show that increases in the precursor concentration allow the production of larger particles. For the case of temperature of 900°C, the increment of particle size is in a good agreement with theoretical analysis result. Small differences are due to the existence of sintering phenomenon during the spray-pyrolysis process. However, for the case of samples prepared with temperature of 1200°C, the trend in particle size is far from theoretical analysis. This deviation is due to the existence of WO_3 material evaporation phenomena. In addition, when using high concentration at 1200°C, sizes of particles are near to that of theoretical results. There are some heat transfer problems during the spray pyrolysis process, making evaporation of WO_3 material incomplete.

Investigation of Effect of Particle Size on Photocatalytic Performance

Photodegradation of RhB using various sizes of particles is shown in Figure 9. The RhB concentration gradually decreased with increasing processing time (shown in solid lines), while the RhB was stable in the absence of a catalyst (shown in a dotted line). The lost RhB concentrations after 1-h photocatalytic process were from 12 to 15%, when using catalyst with a mean size of from 767 to 388 nm, respectively. The rate of photocatalysis (k) was the fastest for particles with a mean size of 388 nm ($k = 1.3672$ min^{-1}) and the slowest for particles with a mean size of 767 nm ($k = 0.9254$ min^{-1}). Particles with a mean size of between 388 and 767 nm had intermediate photodecomposition rates, in which particles with a mean size of 454 and 579 nm had a k value of 1.2637 and 1.1397 min^{-1}, respectively.

The crystal phase of all catalysts were the same (shown in Figure S6 in the Supporting Information), indicating that the fundamental reason for the different photocatalytic behaviors was due to the effect of the particle size. In the same weight of photocatalysts used in the tests, the particle number increases with the decrease of particle size. This condition will be followed by the increase of total surface area of the

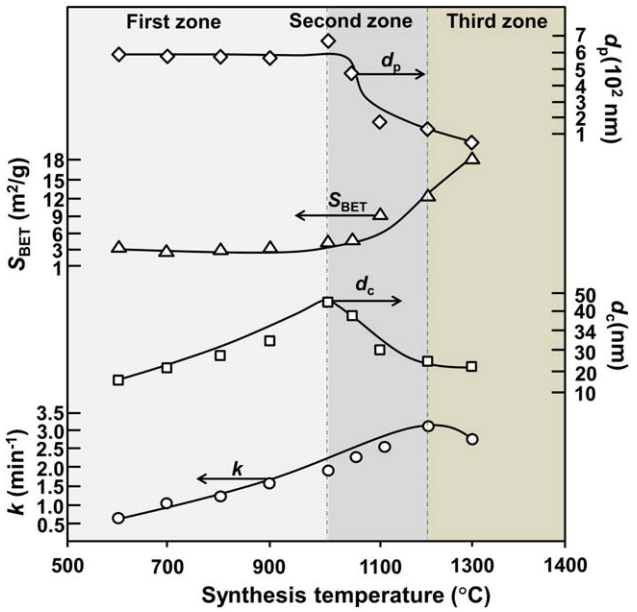

Figure 11. Effect of synthesis temperatures on particle sizes (d_p), surface area (S_{BET}), crystallite sizes (d_C), and photodecomposition rates (k).

[Color figure can be viewed in the online issue, which is available at wileyonlinelibrary.com.]

catalyst. Detailed explanation of the correlation of particle size and surface area is reported in our previous work.[3]

Investigation of Effect of Crystallite Size on Photocatalytic Performance

Photodegradation of RhB as the effect of crystallite size of particles is shown in Figure 10. Similar to above photodecomposition analysis in Figure 9, the RhB concentration gradually decreased with increasing processing time (shown in solid and dashed lines), while RhB was stable in the absence of a catalyst (shown in a dotted line). We found that increases in crystallite size caused increasing of photodegradation rate. The lost RhB concentration after 1-h photocatalytic process were from 8 to 34%, when using catalyst synthesized using temperature of from 600 to 1200°C. However, the lost RhB concentration was 27% when using catalyst synthesized using temperature 1300°C. The improvement of photocatalytic activity was probably because the larger crystallite size results in the more number of active sites in the catalyst. However, we found anomaly for the case of samples prepared with higher temperatures (shown as dashed lines).

Figure 11 shows the detail correlations of synthesis temperature, particle size (d_p), surface area (S_{BET}), crystallite size (d_c), and kinetic photodecomposition rate (k). To clarify the discussion, the figure is divided into three zones, based on the synthesis temperature (1) 600–1000°C (the first zone), (2) 1000–1200°C (the second zone), and (3) above 1200°C (the third zone).

In the first zone, increasing synthesis temperature corresponds to an increase of both crystallite size and photocatalytic activity. The particles size and the surface area are constant. Therefore, the correlation between crystallite size and photocatalytic activity can be investigated directly. It confirms that the ability of catalyst to decompose RhB increases due to increasing crystallite size.

In the second zone, both particle size and crystal size increase with the increasing of the synthesis temperature. Although the crystal size decreases, the photocatalytic activity increases. As explained in Figure 5, using high temperature of above 1000°C causes a reduction of both crystallite and particle sizes. In general, increase of temperature process leads the production of nanoparticles (shown in Figures 3 and 4), in which the use of nanoparticles gives additional factors (i.e., surface area) for the improvement of photodegradation process.

In the third zone, although particle sizes decreases, photocatalytic activity decreases slightly. This may reflect the reason in dominancy of slight decrease in crystallite size for decreasing photocatalytic performance.

In addition, the crystal size at 1300°C is similar to that at 700°C. However, the photocatalytic performances of both particle types were different. This is because of the different specific surface area of both particles.

From the aforementioned results, the optimum synthesis temperature to produce the catalyst with the highest photocatalytic activity was 1200°C and using a precursor concentration of 10 mmol/L. It is also found that the synthesis temperature has a more significant effect than that precursor concentration. However, in addition to both factors, the crystal phase and structure are also influencing the photocatalytic performance. For this reason, the further studies (e.g., crystal phase and pattern, additional doping, etc.) are needed for clarifying how to improve photocatalyst. We believe that insights gained from this type of research will contribute to more fabrication innovation.

Conclusions

The studies on the controllable crystallite and particle sizes of WO_3 particles prepared by a spray-pyrolysis method and their photocatalytic performance have been reported. We controlled the crystallite (from 18 to 50 nm) and particle sizes (from 58 to 677 nm), by changing the synthesis temperature in wide range (120–1200°C) and initial precursor concentration (2.5–15 mmol/L). The capability of photocatalyst can be optimized by changing both the crystallite and the particle sizes. The optimum condition to produce the highest photocatalytic performance of WO_3 particles was at the temperature of 1200°C (crystal size: 25 nm), and initial concentration 10 mmol/L (particle size: 105 nm). The proposal mechanism was also reported to support the level of control over crystallite/particle size by the spray-pyrolysis method. Hopefully, this report is useful for synthesis of particles, particularly with a view to screening and enhancing the material properties.

Acknowledgments

O.A. acknowledges support from Japan Student Services Organization (JASSO) and Kumahira Scholarship and Cultural Foundation. A.B.D.N. acknowledges support from a Japan Society for the Promotion of Science (JSPS) Fellowship (Grant-in-Aid for Scientific Research, No. 2300107000). This research was supported by a Grant-in-Aid for Scientific Research (A) (No. 22246099) and Grant-in-Aid for Young Scientists (B) (No. 23760729) sponsored by the Ministry of Education, Culture, Sports, Science and Technology (MEXT) of Japan.

Literature Cited

1. Bhatkhande DS, Pangarkar VG, Beenackers AA. Photocatalytic degradation for environmental applications-a review. *J Chem Technol Biotechnol*. 2002;77:102–116.
2. Bertus L, Duta A. Synthesis of WO3 thin films by surfactant mediated spray pyrolysis. *Ceram Int*. 2012;38:2873–2882.
3. Nandiyanto ABD, Arutanti O, Ogi T, Iskandar F, Kim TO, Okuyama K. Synthesis of spherical macroporous WO_3 particles and their high photocatalytic performance. *Chem Eng Sci*. 2013.In press.
4. Zheng H, Ou JZ, Strano MS, Kaner RB, Mitchell A, Kalantar-zadeh K. Nanostructured tungsten oxide-properties, synthesis, and applications. *Adv Func Mater*. 2011;21:2175–2196.
5. Lei H, Tang Y-J, Wei J-J, Li J, Li X-B, Shi H-L. Synthesis of tungsten nanoparticles by sonoelectrochemistry. *Ultrason Sonochem*. 2007;14:81–83.
6. Wang F, Li C, Yu JC. Hexagonal tungsten trioxide nanorods as a rapid adsorbent for methylene blue. *Sep Purif Technol*. 2012;91: 103–107.
7. Pokhrel S, Birkenstock J, Schowalter M, Rosenauer A, Mädler L. Growth of ultrafine single crystalline WO3 nanoparticles using flame spray pyrolysis. *Cryst Growth Des*. 2009;10:632–639.
8. Lin H-C, Su C-Y, Yang Z-K, Lin C-K, Ou K-L. A facile route to tungsten oxide nanomaterials with controlled morphology and structure. *Particuology*. 2011;9:517–521.
9. Hong SJ, Jun H, Borse PH, Lee JS. Size effects of WO3 nanocrystals for photooxidation of water in particulate suspension and photoelectrochemical film systems. *Int J Hydrogen Energ*. 2009;34:3234–3242.
10. Boulova M, Lucazeau G. Crystallite nanosize effect on the structural transitions of WO3 studied by raman spectroscopy. *J Solid State Chem*. 2002;167:425–434.
11. Morales W, Cason M, Aina O, de Tacconi NR, Rajeshwar K. Combustion synthesis and characterization of nanocrystalline WO3. *J Am Chem Soc*. 2008;130:6318–6319.
12. Huang R, Shen Y, Zhao L, Yan M. Effect of hydrothermal temperature on structure and photochromic properties of WO3 powder. *Adv Powder Technol*. 2012;23:211–214.
13. Hidayat D, Purwanto A, Wang W-N, Okuyama K. Preparation of size-controlled tungsten oxide nanoparticles and evaluation of their adsorption performance. *Mater Res Bull*. 2010;45:165–173.
14. Purwanto A, Widiyandari H, Ogi T, Okuyama K. Role of particle size for platinum-loaded tungsten oxide nanoparticles during dye photodegradation under solar-simulated irradiation. *Catal Commun*. 2011;12:525–529.
15. Nandiyanto ABD, Okuyama K. Progress in developing spray-drying methods for the production of controlled morphology particles: From the nanometer to submicrometer size ranges. *Adv Powder Technol*. 2011;22:1–19.
16. Wang W-N, Widiyastuti W, Ogi T, Lenggoro IW, Okuyama K. Correlations between crystallite/particle size and photoluminescence properties of submicrometer phosphors. *Chem Mater*. 2007;19:1723–1730.
17. Okuyama K, Shimada M, Adachi M, Tohge N. Preparation of ultrafine superconductive Bi-Ca-Sr-Cu-O particles by metalorganic chemical vapor deposition. *J Aerosol Sci*. 1993;24:357–366.

Manuscript received Apr. 24, 2013, and revision received July 24, 2013, and final revision received Sept. 10, 2013.